Theoretical and Experimental Studies of Active Vibration Control for Beams Using Pole Placement Method

YANG Shaoxuan, *HU Yu*, *SONG Zhiguang**

College of Aerospace and Civil Engineering, Harbin Engineering University, Harbin 150001, P.R. China

Abstract: The vibration control in the frequency domain is significant. Therefore, an active vibration control in frequency domain is studied in this paper. It is generally known that piezo-intelligent structures possess satisfactory performances in the area of vibration control, and macro-fiber composites（MFCs）with high sensitivity and deformability are widely applied in engineering. So, this paper uses the MFC patches and designs a control method based on the pole placement method, and the natural frequency of the beam can be artificially designed. MFC patches are bonded on the top and bottom surfaces of the beam structure to act as the actuators and sensors. Then, the finite element method（FEM）is used to formulate the equation of motion, and the pole placement based on the out-put feedback method is used to design the active controller. Finally, the effectiveness of the active control method is verified.

Key words： piezo-intelligent; macro-fiber composite（MFC）; pole placement; closed-loop control; finite element method（FEM）

0 Introduction

Vibration is a natural phenomenon, which is very common in the field of engineering. The structure exposed to vibration in the long term may cause damage of precision instrument even endanger the structural stability. As a result, vibration control has always been an important challenge in engineering field. Ordinarily, vibration control is composed of passive and active vibration control.

With the rapid development of intelligent materials, piezoelectric materials have been widely used in vibration control fields[1-3] because of their unique piezoelectric effects. In the past decades, researchers have widely investigated the vibration of beams, plates and shells by using piezoelectric materials as sensors and actuators[4-7]. However, the fragile characteristics of piezoelectric patches limit its application in engineering. In order to overcome this weakness, the macro-fiber composite（MFC）was devel-

oped by NASA Langley Research Center in 1999. Because of the excellent characteristics of flexibility and actuating bending moment, MFC has been widely used in the field of vibration control recently[8-10]. Williams et al.[11-13] carried out a detailed description of the MFC manufacturing process and investigated the nonlinear behavior of tensile, shear and temperature effects of MFC. Zhang et al.[14] studied the structural deformation of isotropic and cross-ply composite laminated thin-walled smart structures bonded with orthotropic MFCs. MFC has an outstanding performance in the field of active control. Lucyna et al.[15] designed a closed-loop system with MFC sensor and actuators and applied to suppress circular plate vibrations. Gao et al.[16] utilized MFC to investigate a new multiple model switching adaptive control algorithm to implement the real time active vibration suppression tests with a new multiple switching strategy. Chai et al.[17] studied

the aerothermoelastic characteristics of composite laminated panels and carried out active flutter control of composite laminated panels with time-dependent boundary conditions in supersonic airflow by using MFC materials. Jia et al.[18] measured vibration data from various sources, including aerospace, automotive, engine, bridge and rail applications, confirmed a finite element model and the FE software to simulate the multiphysical process of piezoelectric vibration energy harvesting, and carried out the dynamic mechanical and electrical behaviors of MFC on carbon fiber composite structures.

In general, the active vibration control mainly uses the control method for the structural vibration. Wu et al.[19] utilized PD and fuzzy control algorithms to build the closed-loop feedback control system. Sohn et al.[20] used MFC actuators to suppress the vibration response of the smart hull structure with linear quadratic Gaussian (LQG) control method. Song et al.[21] investigated the optimal active flutter control of supersonic composite laminated panels with distributed piezoelectric actuators/sensors pairs. Comparing two different controllers, numerical simulations show that the optimal locations obtained by the genetic algorithm (GA) can increase the critical flutter aerodynamic pressure significantly, and the LQG algorithm is more suitable in flutter suppression for supersonic structures than the proportional feedback controller. Through the collection and arrangement of the literature, the general active control method cannot change the dynamic characteristics of the structure itself. The pole placement method possesses such characteristics. It can arbitrarily assign any natural frequency of the structure, and has been widely used in the structural vibration control[22-25]. Tehrani et al.[26] carried out the theory and practical application of the receptance method for vibration suppression in structures by multi-input partial pole placement.

However, most researchers commonly considered vibration control in time domain by using piezoelectric ceramics, but very limited literatures have been found to investigate the active control in frequency domain. This paper creatively investigates a vibration control method in frequency domain which is the pole placement method combined with piezoelectric effect. MFC patches are bonded on the top and bottom surfaces of the beam structure to act as the actuators and sensors. By using the MFC patches and designing the control process through the pole placement method, the natural frequency of the beam can be artificially designed. The effects of active vibration control for beam using pole placement method are carried out through the theoretical, numerical and experimental verifications.

1   Theoretical Formulations

1.1   Structural modeling

MFCs are mainly composed of piezoceramic epoxy matrix and electrodes. Although each of these materials is considered to be isotropic by itself (or transversely isotropic in the case of the poled PZT), the resulting composite behaves in an orthotropic manner when manufactured into a fiber-reinforced lamina[27-28].

There are mainly two types of MFC, i.e., MFC-d_{31} and MFC-d_{33}. MFC-d_{31} is polarized along the thickness direction and perpendicular to the fiber direction. It is usually used as sensors. On the contrary, MFC-d_{33} is polarized along the fiber direction. It may have greater driving force and is usually used as actuators.

A cantilevered beam with MFC patches is shown in Fig.1, where the MFC-d_{31} and MFC-d_{33} patches are bonded on the top and bottom surfaces to act as sensor and actuator, respectively.
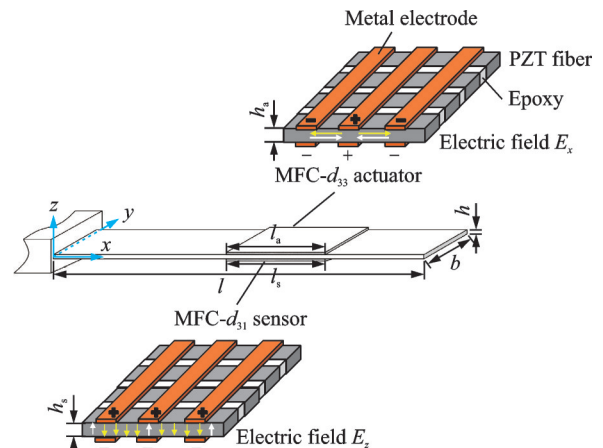
Fig.1   Schematic diagram of the smart structure

To formulate the equation of motion of the structural system, the Hamilton's principle is applied, shown as

$$\int_{t_1}^{t_2} [\delta(T-U)+\delta W] \mathrm{d}t = 0 \qquad (1)$$

where t_1 and t_2 are the integral limits, and T, U and δW the kinetic energy, strain energy and virtual work done by the external forces, calculated by

$$T = \frac{1}{2}\int_{V_b} \rho_b(\dot{w}^2+\dot{u}^2)\mathrm{d}V +$$
$$\frac{1}{2}\int_{V_a+V_s} \rho_P(\dot{w}^2+\dot{u}^2)\mathrm{d}V \qquad (2)$$

$$U = \frac{1}{2}\int_{V_b} \boldsymbol{\varepsilon}_x^{\mathrm{T}}\sigma_b \mathrm{d}V + \frac{1}{2}\int_{V_a+V_s} \boldsymbol{\varepsilon}_x^{\mathrm{T}}\sigma_P \mathrm{d}V -$$
$$\frac{1}{2}\int_{V_a} \boldsymbol{E}^{\mathrm{T}} D_a \mathrm{d}V \qquad (3)$$

$$\delta W = F_0 \delta w(x_F) \qquad (4)$$

where dot denotes the derivative with respect to time; ρ_b is the density of base beam; ρ_P the density of MFC, in which sensor and actuator have the same mass density; F_0 the external load; x_F the coordinates of F_0; $\boldsymbol{\varepsilon}_x$ the strain of beam and MFC (assuming that the MFC is fully bonded to the beam, and they can be considered to have the same strain); E the electric field; D_a the electric displacements of MFC actuator; σ_b and σ_P are the stress of beam and MFC; and V_b, V_a and V_s the volume of the beam, actuators and sensors, respectively. The in-plane and transverse displacements in the above equations are given out according to the Euler-Bernoulli beam theory, shown as

$$u = -z\frac{\partial w}{\partial x} \qquad (5)$$

where w indicates the transverse displacement along the x direction and u the in-plane displacement.

For the beam structure, it can be regarded as a one-dimensional model. While for MFC-d_{33}, the electric field is only applied to the polarization direction. The constitutive equation can be shown as

$$\sigma_s = E_s\boldsymbol{\varepsilon}_x, \ D_z^s = d_{31}\sigma_s \,(\text{for MFC-}d_{31}\text{ sensor}) \quad (6)$$
$$\sigma_a = E_a(\boldsymbol{\varepsilon}_x - d_{33}E_x) \qquad (7)$$
$$D_x^a = d_{33}\sigma_a + \boldsymbol{\varepsilon}_{33}E_x \,(\text{for MFC-}d_{33}\text{ actuator}) \quad (8)$$

where $\boldsymbol{\varepsilon}_x = -z\partial^2 w/\partial x^2$; $E_x = V(t)/h_a$ is the electric field in the x direction, here $V(t)$ the external applied voltage; $\boldsymbol{\varepsilon}_{33}$ the permittivity coefficient of the

MFC; E_b, E_s and E_a are the Young's modulus of the base beam, MFC-d_{31} and MFC-d_{33}; and d_{31} and d_{33} the piezoelectric coefficients.

According to the FEM, the displacement field can be expressed in terms of interpolation functions and nodal coordinates, shown as

$$w(x,t) = \boldsymbol{N}^{\mathrm{T}}(x)\boldsymbol{q}_e(t) \qquad (9)$$

where $\boldsymbol{N}(x)$ and $\boldsymbol{q}_e(t)$ are the column vectors of interpolation functions and nodal coordinates. For the thin beam structure, a two-node Euler beam element is used. The interpolation function and nodal coordinate vector are

$$\boldsymbol{q}_e = [\ w_1 \ \ \theta_1 \ \ w_2 \ \ \theta_2\ ]^{\mathrm{T}} \qquad (10)$$
$$\boldsymbol{N} = [\ 1-3\zeta^2+2\zeta^3 \ \ \ l_e(\zeta-2\zeta^2+\zeta^3) \ \ \ 3\zeta^2-2\zeta^3$$
$$l_e(-\zeta^2+\zeta^3)\ ]^{\mathrm{T}} \qquad (11)$$

where $\theta_i = \partial w_i/\partial x$; l_e is the length of element; $\zeta = (x-x_1)/l_e$ the normalized coordinate; x_1 the coordinates of the node on the left end of the element.

Thus, based on the Hamilton principle, the equation of motion can be obtained as

$$\boldsymbol{M}_e\ddot{\boldsymbol{q}}_e(t)+\boldsymbol{K}_e\boldsymbol{q}_e(t)+\boldsymbol{K}_{ae}V_i(t) = \boldsymbol{F}_e \qquad (12)$$

where $\boldsymbol{M}_e$ and $\boldsymbol{K}_e$ are the element structural mass and stiffness matrices; $\boldsymbol{K}_{ae}$ is the electromechanical vector; $V_i(t)$ the input voltage generated by the ith MFC-d_{31} actuator; and $\boldsymbol{F}_e$ the element external force vector. They are calculated by

$$\boldsymbol{M}_e = (\rho_b A_b + \delta_s\rho_s A_s + \delta_a\rho_a A_a)l_e\int_0^1 \boldsymbol{N}\boldsymbol{N}^{\mathrm{T}}\mathrm{d}\zeta \quad (13)$$

$$\boldsymbol{K}_e = (E_b I_b + \delta_a E_a I_a + \delta_s E_s I_s)\frac{1}{l_e^3}\int_0^1 \frac{\partial^2 \boldsymbol{N}}{\partial\zeta^2}\frac{\partial^2 \boldsymbol{N}^{\mathrm{T}}}{\partial\zeta^2}\mathrm{d}\zeta$$
$$(14)$$

$$\boldsymbol{K}_{ae} = \frac{(h_b+h_a)E_a d_{33}}{2l_e}\int_0^1 \frac{\partial^2 \boldsymbol{N}^{\mathrm{T}}}{\partial\zeta^2}\mathrm{d}\zeta \qquad (15)$$

where A_b, A_s and A_a are the cross-section area of base beam, MFC sensor and actuator, respectively; δ_s and δ_a can be equal to 1 or 0 depending on whether the structure contains the sensor or actuator layers, and

$$\begin{cases} I_b = \dfrac{1}{12} b h_b^3 \\[2mm] I_a = b_a\left(\dfrac{1}{4}h_b^2 h_a + \dfrac{1}{2}h_b h_a^2 + \dfrac{1}{3}h_a^3\right) \\[2mm] I_s = b_s\left(\dfrac{1}{4}h_b^2 h_s + \dfrac{1}{2}h_b h_s^2 + \dfrac{1}{3}h_s^3\right) \end{cases} \qquad (16)$$

For MFC sensors, according to the Gauss law, the closed-circuit charge of the ith MFC sensor measured through the electrodes is

$$Q_{se}^{(i)}=\frac{b_s}{2}\left[\int_{l(z=-h_b/2)}D_z^s\mathrm{d}x+\int_{l(z=-h_b/2-h_s)}D_z^s\mathrm{d}x\right]=$$

$$\frac{b_sE_sd_{31}(h_b+h_s)}{2l_e}\int_0^1\frac{\partial^2N^\mathrm{T}}{\partial\zeta^2}\mathrm{d}\zeta=\hat{K}_{se}^\mathrm{T}q_e \quad (17)$$

where b_s is the width of the MFC sensor. And the sensing voltage is expressed as

$$V_{se}^{(i)}(t)=\frac{h_s}{\varepsilon_rl_sb_s}Q_{se}^{(i)}=\frac{h_s}{\varepsilon_rl_sb_s}\hat{K}_{se}^\mathrm{T}q_e=$$

$$\frac{E_sd_{31}h_s(h_b+h_s)}{2\varepsilon_{33}l_sl_e}\int_0^1\frac{\partial^2N^\mathrm{T}}{\partial\zeta^2}\mathrm{d}\zeta=K_{se}^\mathrm{T}q_e \quad (18)$$

Based on the above mass and stiffness matrices and considering the boundary condition, after assembling, the global equation of motion can be obtained as

$$M\ddot{q}(t)+Kq(t)+K_aU(t)=F \quad (19)$$

$$V_s^{(i)}(t)=K_{si}^\mathrm{T}q \quad (20)$$

where M and K are the global mass and stiffness matrices, and $U(t)=[\,V_1(t) \quad V_2(t) \quad \cdots \quad V_p(t)\,]^\mathrm{T}$.

1. 2　Pole placement design

To conduct the pole placement control, the equation of motion in modal space should be transformed to state space as

$$\dot{Z}(t)=\begin{Bmatrix}\dot{q}\\\ddot{q}\end{Bmatrix}=\begin{bmatrix}0 & I\\-M^{-1}K & 0\end{bmatrix}\begin{Bmatrix}q\\\dot{q}\end{Bmatrix}+$$

$$\begin{bmatrix}0\\-M^{-1}K_a\end{bmatrix}U(t)=AZ(t)+BU(t) \quad (21)$$

$$Y(t)=[\,V_s^{(1)} \quad V_s^{(2)} \quad \cdots \quad V_s^{(p)}\,]^\mathrm{T}=$$

$$\begin{bmatrix}K_{s1}^\mathrm{T} & 0 & 0 & \cdots & 0\\K_{s2}^\mathrm{T} & 0 & 0 & \cdots & 0\\\vdots & \vdots & \vdots & \ddots & 0\\K_{sp}^\mathrm{T} & 0 & 0 & \cdots & 0\end{bmatrix}\begin{Bmatrix}q\\\dot{q}\end{Bmatrix}=CZ(t) \quad (22)$$

where $A\in\mathrm{R}^{2n\times2n}$, $B\in\mathrm{R}^{2n\times p}$, $C\in\mathrm{R}^{p\times2n}$.

Based on the output feedback system, the control input voltage is expressed as

$$U(t)=-G_0Y(t)=-G_0CZ(t) \quad (23)$$

where $G_0\in\mathrm{R}^{p\times p}$ is the matrix of feedback control gain. Therefore, the closed-loop system becomes

$$\dot{Z}(t)=(A-BG_0C)Z(t) \quad (24)$$

The eigenvalue equation of the closed-loop system can be placed in following equation

$$\Delta_c(\lambda_c)=\left|\lambda_cI_n-(A-BG_0C)\right|=0 \quad (25)$$

where λ_c is the eigenvalue of the closed-loop system. According to the linear transformation, the eigenvalue equation can be expressed by

$$\Delta_c(\lambda_c)=\left|\lambda_cI_n-A\right|\left|I_p+G_0\varphi(\lambda_c)\right|=0 \quad (26)$$

where

$$\varphi(\lambda_c)=[\,C(\lambda_cI_n-A)^{-1}B\,]\in\mathrm{R}^{p\times p} \quad (27)$$

Since λ_c is the eigenvalue of the closed-loop system, the following equation can be obtained as

$$\left|I_p+G_0\varphi(\lambda_c)\right|=0 \quad (28)$$

Therefore, the matrix G_0 should satisfy the above equation, and it can be obtained by

$$G_0=-e\Gamma^{-1} \quad (29)$$

where

$$\Gamma=\begin{bmatrix}\varphi_{m1}(\lambda_{c1}) & \varphi_{m2}(\lambda_{c2}) & \cdots & \varphi_{mp}(\lambda_{cp})\end{bmatrix} \quad (30)$$

where $\varphi_{mp}(\lambda_{cp})$ represents the mpth column of the matrix $\varphi(\lambda_{cp})$, and correspondingly, the matrix is composed of the corresponding column of the unit matrix I as

$$e=\begin{bmatrix}I_{m1} & I_{m2} & \cdots & I_{mp}\end{bmatrix} \quad (31)$$

1. 3　Decoupling method

For uncoupled state space equation, when poles are placed to the desired poles, the rest poles will also move. As a result, the previous stable system may lose stability. In order to solve this problem, the decoupling of the equation of motion is conducted. The following transformation is introduced

$$Z=\psi\zeta(t) \quad (32)$$

where

$$\psi=[\,a_1 \quad b_1 \quad a_2 \quad b_2 \quad \cdots \quad a_m \quad b_m\,] \quad (33)$$

where $a_j+\mathrm{i}b_j$ $(j=1,2,\cdots,m)$ are m pairs of conjugate complex eigenvectors of the state matrix A. This state transformation matrix can lead to the following relationship

$$\psi^{-1}A\psi=\bigoplus_{j=1}^m\Lambda_j \quad (34)$$

where

$$\Lambda_j=\begin{bmatrix}\gamma_j & \omega_j\\-\omega_j & \gamma_j\end{bmatrix} \quad (35)$$

where γ and ω are the real and imaginary parts of the eigenvalue of A.

Substituting Eq.(32) into Eq.(21), the decoupled state equation can be obtained as

$$\dot{\boldsymbol{\zeta}}(t) = \boldsymbol{\Lambda}\boldsymbol{\zeta} + \hat{\boldsymbol{U}}(t) \tag{36}$$

where $\hat{\boldsymbol{U}} = \boldsymbol{\psi}^{-1}\boldsymbol{B}\boldsymbol{U}$.

Based on the decoupling state space equation of motion, and the pole placement method given in Eq.(29), the matrix of feedback control gain can be obtained as

$$\boldsymbol{G} = \begin{pmatrix} G_1 & \cdots & 0 & 0 & \cdots & 0 \\ 0 & \ddots & 0 & 0 & \ddots & 0 \\ 0 & \cdots & G_i & 0 & \cdots & 0 \\ 0 & 0 & 0 & 0 & \cdots & 0 \\ \vdots & \ddots & \vdots & \vdots & \ddots & \vdots \\ 0 & \cdots & 0 & 0 & \cdots & 0 \end{pmatrix} \tag{37}$$

2 Numerical Results and Discussion

In the numerical simulations, the cantilever beam is made of steel 304 whose geometrical sizes are $l = 0.25$ m, $b = 0.02$ m, $h_b = 0.001$ m, $E_b = 210$ GPa, $\rho_b = 7\,850$ kg/m^3, and $\nu_b = 0.3$. M2814-P1 is adopted as actuator and M2814-P2 is adopted as sensor. Their parameters are 38 mm×20 mm×0.3 mm, and the actuating size is 28 mm×14 mm×0.3 mm. MFC patches arranged in the up-and-down surfaces are pasted with epoxy resin glue at a distance of 0.09 m away from the fixed end. The relevant material properties are given in Table 1.

Table 1   Relevant material property specifications

Property	MFC-d_{31}	MFC-d_{33}
Elastic modulus E/GPa	30.336	15.857
Density ρ/(kg·m^{-3})	5.44	5.44
Piezoelectric constant d_{31}/(m·V^{-1})	-1.7×10^{-10}	—
Piezoelectric constant d_{33}/(m·V^{-1})	—	4×10^{-10}
Dielectric coefficient ε_{33}/(nF·m^{-1})	—	1.73×10^{-8}

In the experiment, the mass of the acceleration sensor cannot be ignored. Therefore, the acceleration sensor is replaced by an additional mass about 7.85 g. Before the active control, the natural frequencies of the structure are verified. The comparison results are shown in Table 2. It can be seen that the three results agree well with each other, which verifies the correctness of the formulations and experiment.

Table 2   Comparison of natural frequencies obtained by different methods   Hz

Frequency	f_1	f_2	f_3
Present result	15.94	122.60	354.50
Experimental result	16.60	123.05	354.26
COMSOL result	15.79	120.54	358.33

2.1 Closed-loop control

Based on the above verification, the active control is carried out. The schematic diagram is displayed in Fig.2. It can be seen that the MFC patches are bonded on the upper and lower surfaces with the epoxy resin glue. By this way, the structure can effectively realize the mutual conversion between voltage and displacement.
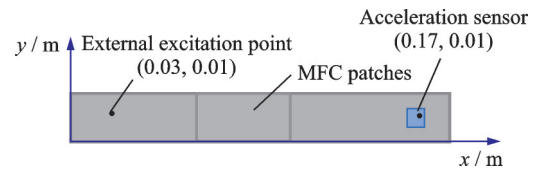
Fig.2   Positions of external excitation, MFC patches and acceleration sensor

Under the closed-loop control, the sensor is responsible for converting the displacement into the induced voltage and acting on the actuator with a certain gain. Considering the piezoelectric effect of piezoelectric materials, the stiffness of the beam can be changed, and as a result, the natural frequencies can be changed.

Experimental devices shown in Fig.3 can be divided into four parts, i.e., the control system, data acquisition system, excitation system and boundary condition device. The control system is composed of dSpace MicroLabBox, voltage amplifier and Computer 1. Its main function is to collect the induced voltage generated by the MFC sensor and output voltage to MFC actuator. The data acquisition system consists of Computer 2 and data acquisition equipment. The data acquisition equipment is used to collect the displacement signal generated by the acceleration sensor and perform Fourier transform on the signal. External excitation includes a vibration exciter and a power amplifier. The boundary condition device is displayed in Fig.4.
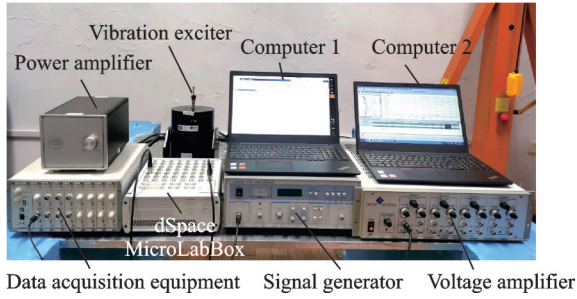
Fig.3   Experiment apparatuses
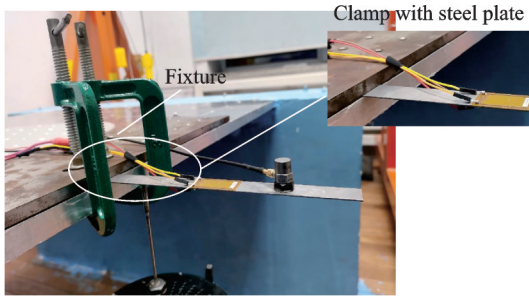
Fig.4   Boundary condition

Firstly, the influences of the closed-loop control on the natural frequency are investigated. Based on output feedback, different values of control gains are adopted in the experiment. In this paper, the control gain in the experiment is verified by the theoretical calculation. The excitation system is set to be sweep frequency in the range of 0—200 Hz.

The results of Figs.5, 6 show that the theoretical results agree well with the experimental results, and the natural frequency increases with the increase of the control gain. Contrary to Figs.5, 6, Figs.7, 8 show a decreased trend of natural frequency of the beam under negative control gain. The theoretical results are also coincident with the experimental results.

With the increase of the control gain, the control effects become more obvious. As shown in Figs.9—11, the experimental results still agree well with the theoretical calculations with the increase of the control gain. The results show that the closed-loop experiment can realize the change of low-order natural frequency up to 20 Hz. In other words, the vibration characteristics of the structure can be improved by closed-loop control method in practical application.
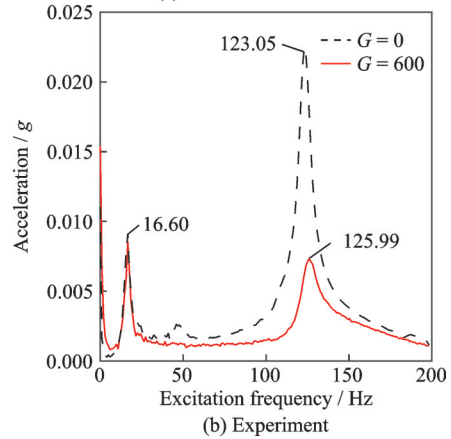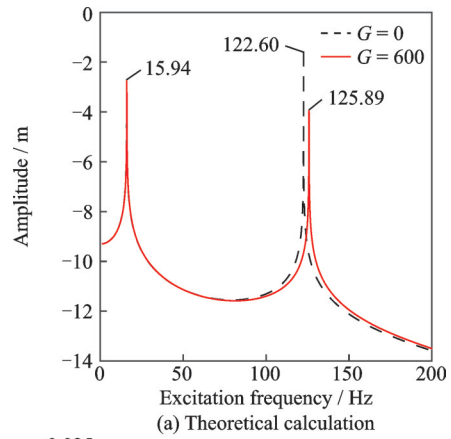
Fig.5   Comparisons of the controlled natural frequencies when $G=600$ and without control
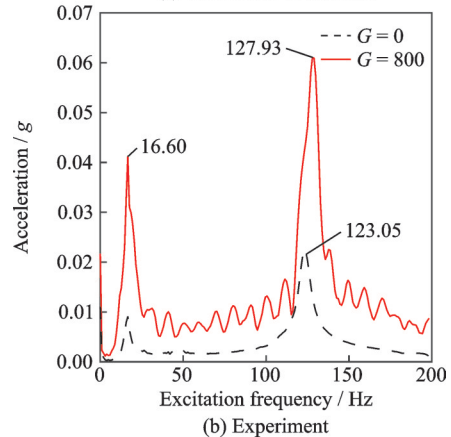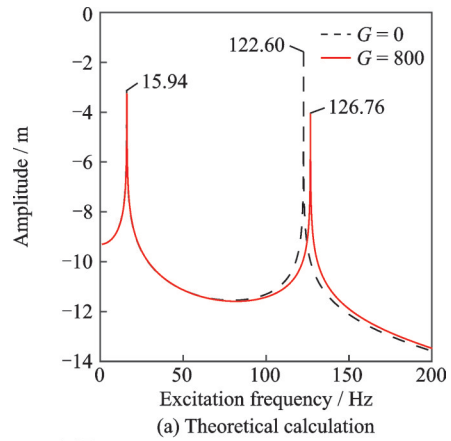
Fig.6   Comparisons of the controlled natural frequencies when $G=800$ and without control
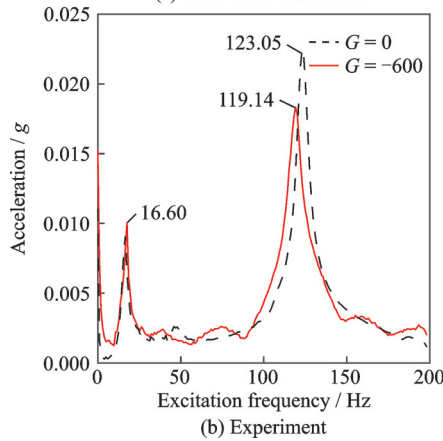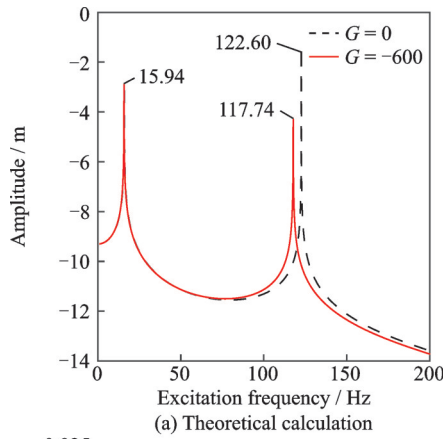
Fig.7   Comparisons of the controlled natural frequencies when $G=-600$ and without control

Fig.8   Comparisons of the controlled natural frequencies when $G=-800$ and without control
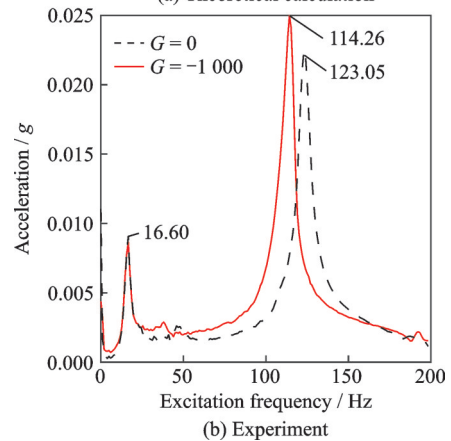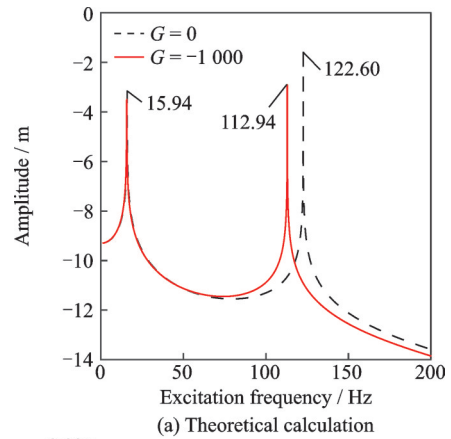
Fig.9   Comparisons of the controlled natural frequencies when $G=-1\,000$ and without control
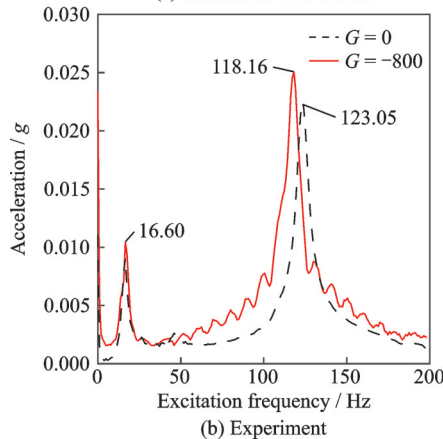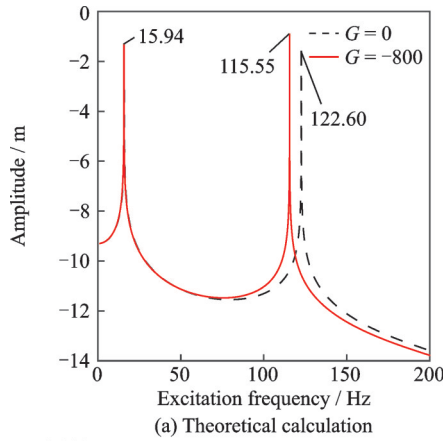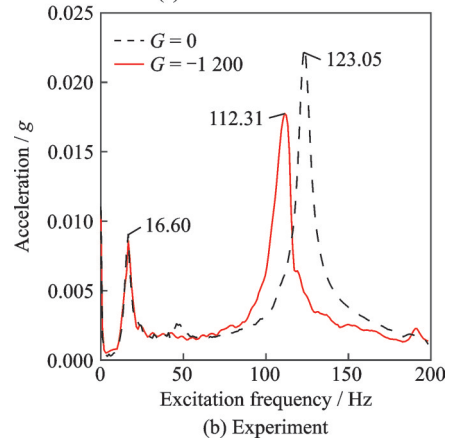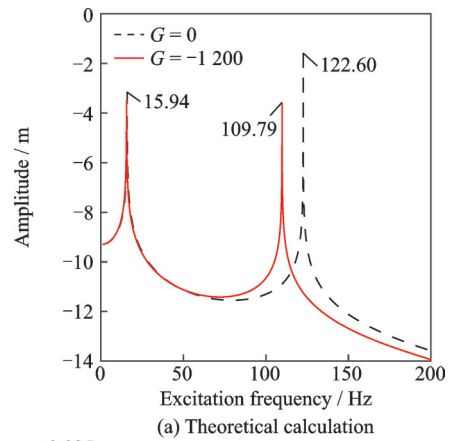
Fig.10   Comparisons of the controlled natural frequencies when $G=-1\,200$ and without control

(a) Theoretical calculation

(b) Experiment
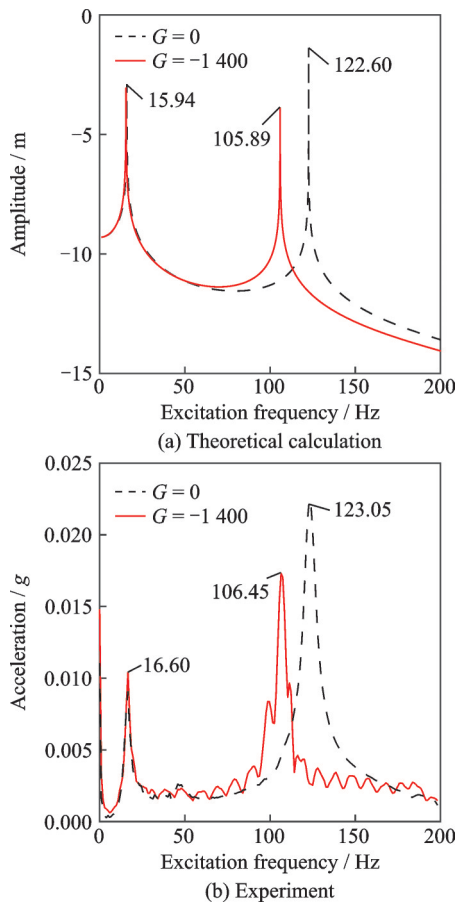
Fig.11   Comparisons of the controlled natural frequencies when $G=-1\,400$ and without control

2. 2   Pole placement control

Poles represent the eigenvalues of structure system. They are always composed of real and imaginary components, and can be expressed by $\lambda_{1,2} = -\zeta\omega_0 \pm \omega_0(\zeta^2-1)^{1/2}$. The real part reflects the damping characteristics of the structure, and the imaginary part is related to the vibration frequency of the structure. By changing the value of system poles, the effect of changing a certain order of natural frequency can be realized.

Since only one pair of MFC actuator and sensor is used in the theoretical and experimental studies, only one pair of poles can be controlled.

For the structural system studied in this paper, the open-loop poles are $\lambda_{1,2} = \pm 2\pi \times 15.94\mathrm{i}$. Limited by experimental and equipment conditions, the pole is going to be controlled to $\lambda_{1,2} = \pm 2\pi \times 15.50\mathrm{i}$ in the experiment. Based on the pole placement control method, the feedback control gain is $G = 1.314\mathrm{e}^{-3}$. The theoretical and experimental results

are shown in Fig.12. It can be seen that the two results agree well with each other, which indicates the correctness of the theoretical analysis.

(a) Theoretical calculation
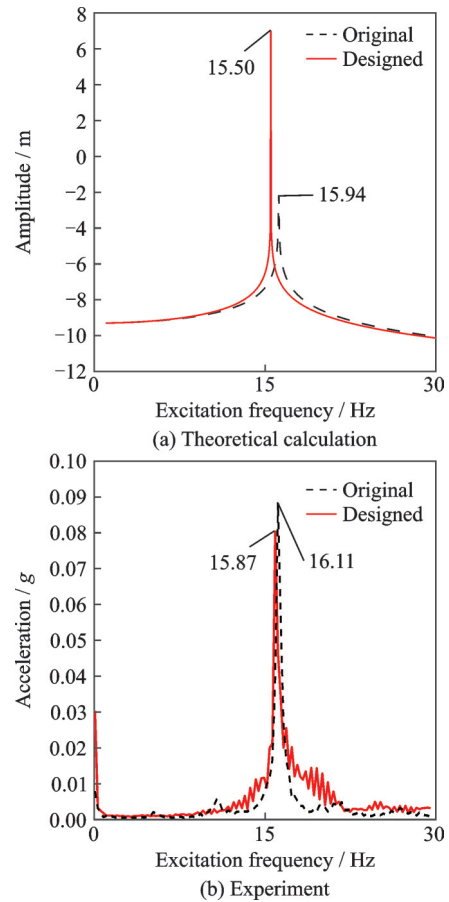
(b) Experiment

Fig.12   Theoretical and experimental results controlled by the pole placement method

Based on the above verification, the pole placement method is used to investigates the active control effect on the first natural frequency, and the results are shown in Figs.13—16.
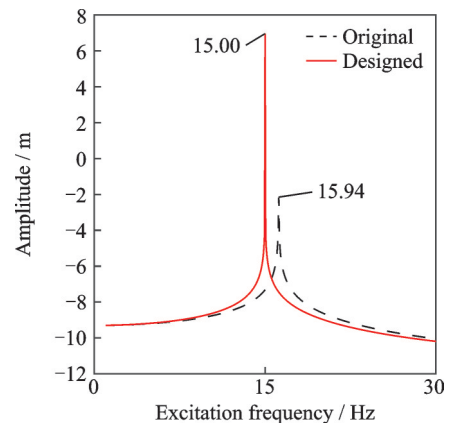
Fig.13   Natural frequencies controlled to 15 Hz with $G=-1\,572$ and without control
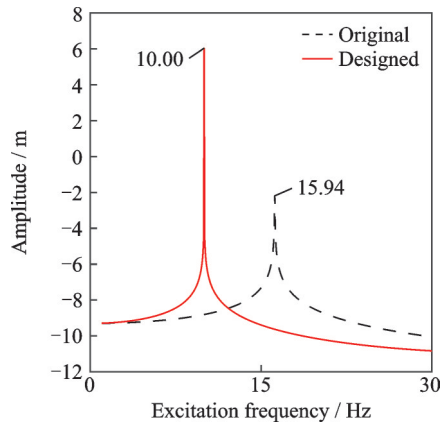
Fig.14   Natural frequencies controlled to 10 Hz with $G=-2\,319$ and without control
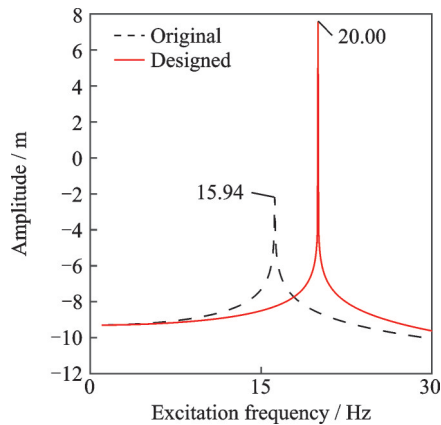
Fig.15   Natural frequencies controlled to 20 Hz with $G=-2\,721$ and without control
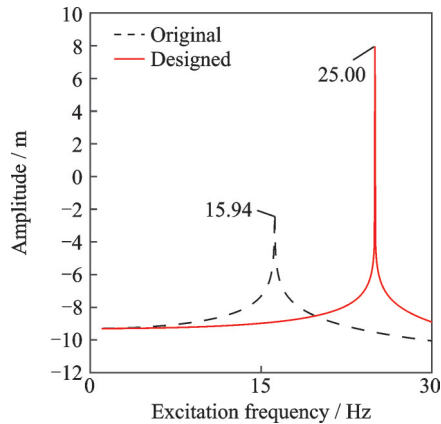
Fig.16   Natural frequencies controlled to 25 Hz with $G=-2\,565$ and without control

2.3   Decoupled pole placement control

When conducting the pole placement control, although the certain natural frequency can be controlled, other poles may also be changed at the same time, which can be observed from Table 3. When the first order of natural frequency is controlled to 10 Hz, the second and third orders of natural frequencies are also changed. To solve this prob-

lem, the control equation is decoupled. It can be seen from Table 3 that after decoupling, only the first natural frequency is changed and the other two frequencies remain unchanged. The other four desired natural frequencies are also considered, and the results are shown in Tables 4—6.

Table 3   Comparisons of the natural frequencies controlled to 10 Hz   Hz

Frequency	f_1	f_2	f_3
Without control	15.94	122.60	354.50
Coupled	10.00	59.86	347.75
Decoupled	10.00	122.60	354.50

Table 4   Comparisons of the natural frequencies controlled to 15 Hz   Hz

Frequency	f_1	f_2	f_3
Without control	15.94	122.60	354.50
Coupled	15.00	96.15	351.35
Decoupled	15.00	122.60	354.50

Table 5   Comparisons of the natural frequencies controlled to 25 Hz   Hz

Frequency	f_1	f_2	f_3
Without control	15.94	122.60	354.50
Coupled	25.00	0+40.86i	351.35
Decoupled	25.00	122.60	354.50

Table 6   Comparisons of the natural frequencies controlled to 50 Hz   Hz

Frequency	f_1	f_2	f_3
Without control	15.94	122.60	354.50
Coupled	1.79	50.00	351.35
Decoupled	50.00	122.60	354.50

It can be seen from Tables 5 and 6 that serious problems occur in the situation of without decoupled system. Table 5 shows the structural instability problem. And Table 6 shows that although the target natural frequency is obtained, the first natural frequency is replaced by other values. The above examples prove the decoupling method is very effective in the pole placement for the active vibration control.

3   Conclusions

The piezoelectric material is used to conduct the active vibration control. Theoretically, the natural frequency can be changed by adjusting the feedback control gains. Numerical calculations and ex-

periments verified this conclusion. The equation of motion is formulated by the Hamilton principle and the finite element method. In the experiment, the correctness of the closed-loop control is verified in the frequency domain. Moreover, the control effect of the pole placement method is investigated through the theoretical and experimental analyses. Based on the results, the following conclusion can be drawn.

(1) The closed-loop control and pole placement method based on the output feedback is effective in practical application.

(2) The core of this active vibration control method is to change the natural frequencies of structure arbitrarily.

(3) The decoupled state equation can achieve the independence of poles from unplaced and placed, which can effectively avoid the instability of system.

References

[1] BAILEY T, HUBBARD J E. Distributed piezoelectric-polymer active vibration control of a cantilever beam[J]. Journal of Guidance, Control, and Dynamics, 1985,8: 605-611.

[2] TSUSHIMA N, SU W H. A study on adaptive vibration control and energy conversion of highly flexible multifunctional wings[J]. Aerospace Science and Technology, 2018, 79: 297-309.

[3] SHEN X, HUANG Y, ZHANG L, et al. Piezoelectric vibration control in wind tunnel tests[J]. Transactions of Nanjing University of Aeronautics, 2021, 38 (3): 437-449.

[4] LIN J C, NIEN M H. Adaptive modeling and shape control of laminated plates using piezoelectric actuators[J]. Journal of Materials Processing Technology, 2007,189(1/2/3): 231-236.

[5] HWANG W S, HWANG W B, PARK H C. Vibration control of laminated composite plate with piezoelectric sensor/actuator: Active and passive control methods[J]. Mechanical System and Signal Processing, 1994, 8(5): 571-583.

[6] CHEN T, WANG Y Q, YANG Z, et al. Release method of microobjects based on piezoelectric vibration[J]. Transactions of Nanjing University of Aeronautics, 2017, 34(1): 37-42.

[7] CHUNG J, LIM H, LIM M, et al. Object classification based on piezoelectric actuator-sensor pair on robot hand using neural network[J]. Smart Materials and Structures, 2020, 29(10): 105020.

[8] BINETTE P, DANO M, GENDRON G. Active shape control of composite structures under thermal loading[J]. Smart Material and Structure, 2009, 18 (2): 025007.

[9] TU J W, ZHANG J R, ZHU Q Y, et al. The actuation equation of macro-fiber composite coupled plate and its active control over the vibration of plate and shell[J]. Structural Monitoring and Maintenance, 2017, 5(2): 297-311.

[10] RIMASAUSKIENE R, JURENAS V, RADZIENSKI M, et al. Experimental analysis of active-passive vibration control on thin-walled composite beam[J]. Composite Structures, 2019, 223: 110975.

[11] WILLIAMS R B, GRIMSLEY B W, INMAN D J, et al. Manufacturing and mechanics-based characterization of macro fiber composite actuators[C]//Proceedings of 2002 ASME International Adaptive Structures and Materials Systems Symposium. New Orleans, LA, USA: ASME, 2002.

[12] WILLIAMS R B, INMAN D J, MICHAELW H. Nonlinear tensile and shear behavior of macro fiber composite actuators[J]. Journal of Composite Materials, 2004, 38(10): 855-869.

[13] WILLIAMS R B, INMAN D J, WILKIE W K. Modeling of temperature effects in macro fiber composite actuators[C]//Proceedings of the 14th US National Congress of Theoretical and Applied Mechanics Conference. Blacksburg, VA, US: [s.n.], 2002.

[14] ZHANG S Q, LI Y X, SCHMIDT R. Modeling and simulation of macro-fiber composite layered smart structures[J]. Composite Structures, 2015, 150: 62-72.

[15] LUCYNA L, DOMINIK M. MFC sensors and actuators in active vibration control of the circular plate[J]. Archives of Acoustics, 2015, 40(2): 257-265.

[16] GAO Z Y, HUANG J Q, MIAO Z H, et al. Multiple model switching adaptive control for vibration control of cantilever beam with varying load using MFC actuators and sensors[J]. Smart Structures and Systems, 2020, 25(5): 559-567.

[17] CHAI Y Y, SONG Z G, LI F M, Active aerothermoelastic flutter suppression of composite laminated panels with time-dependent boundaries[J]. Composite Structures, 2017,179: 61-76.

[18] JIA Y, WEI X Y, LIU X, et al. Multiphysics vibration FE model of piezoelectric macro fiber composite on carbon fiber composite structures[J]. Composites Part B: Engineering, 2019, 161: 376-385.

[19] WU C S, XU M L, WU T H, et al. Active vibration control of the panel reflection antenna by MFC sensors and actuators[J]. International Journal of Applied Electromagnetics and Mechanics. 2016, 52: 1267-1275.

[20] SOHN J W, CHOI S B, KIM H S. Vibration control

of smart hull structure with optimally placed piezoelectric composite actuators[J]. International Journal of Mechanical Sciences, 2011,53: 647-659.

[21] SONG Z G, LI F M. Optimal locations of piezoelectric actuators and sensors for supersonic flutter control of composite laminated panels[J]. Journal of Vibration and Control, 2013, 20: 2118-2132.

[22] ARIYATANAPOL R, XIONG Y P, OUYANG H J. Partial pole assignment with time delays for asymmetric systems[J]. Acta Mechanica, 2018, 229: 2619-2629.

[23] LIU T R, CHANG L. Vibration control of wind turbine blade based on data fitting and pole placement with minimum-order observer[J]. Shock and Vibration, 2018, 2018: 5737359.

[24] MASSOULEH S H M, KORDKHEILI S A H, NAVAZI H M, et al. Combining pole placement and online empirical mode decomposition methods to adaptive active control of structural vibration[J]. Journal of Vibration and Acoustics, 2019, 141(4): 014008.

[25] MOKRANI B, BATOU A, FICHERA S, et al. The minimum norm multi-input multi-output receptance method for partial pole placement[J]. Mechanical Systems and Signal Processing, 2019, 129: 437-448.

[26] TEHRANI M G, ELLIOTT R N R, MOTTERSHEADN J E. Partial pole placement in structures by the method of receptances: Theory and experiments[J]. Journal of Sound and Vibration, 2010, 329: 5017-5035.

[27] ZHANG S Q, LI Y X, SCHMIDT R. Modeling and simulation of macro-fiber composite layered smart structures[J]. Composite Structures, 2015, 126: 89-100.

[28] BISCANI F, NASSER H, BELOUETTAR S, et al. Equivalent electro-elastic properties of macro fiber composite (MFC) transducers using asymptotic expansion approach[J]. Composites: Part B, 2011, 42: 444-455.

Authors   Ms. **YANG Shaoxuan** is currently studying for a master's degree at Harbin Engineering University. Her research interests include piezoelectric materials, metamaterial structures and active vibration control.

Prof. **SONG Zhiguang** received the Ph.D. degree in General Mechanics and Mechanics Foundational from Harbin Institute of Technology, Harbin, China, in 2014. He is the winner of the "Youth Project of Overseas High-Level Talent Introduction Program" and a Humboldt scholar in Germany. Now he is the deputy director of the Department of Engineering Mechanics of Harbin Engineering University. His main research interests are aerothermoelasticity, structural vibration control, nonlinear dynamics and computational mechanics.

Author contributions   Prof. **SONG Zhiguang** designed and discussed the study. Ms. **YANG Shaoxuan** complied the models, conducted the analysis, interpreted the results and wrote the manuscript. Mr. **HU Yu** contributed to the experiment analysis and revision of the study. All authors commented on the manuscript draft and approved the submission.

Competing interests   The authors declare no competing interests.

(Production Editor: ZHANG Huangqun)

基于极点配置法的梁振动主动控制理论与实验研究

杨韶瑄，胡　宇，宋智广

(哈尔滨工程大学航天与建筑工程学院,哈尔滨 150001,中国)

摘要：基于频域的振动控制对于结构动力学十分重要,因此本文研究了一种基于极点配置法的频域振动主动控制理论。由于压电智能结构在振动控制领域具有令人满意的性能,并且宏观纤维复合材料(Macro-fiber composite,MFC)具有高灵敏度和可变形性,本文使用 MFC 片并基于极点配置法设计控制方法,可以人为地设计梁的固有频率。研究中 MFC 片被粘结在梁结构的顶面和底面分别作为作动器和传感器。然后采用有限元法建立了智能结构运动方程,并基于输出反馈的极点配置法设计了主动控制器。最后通过实验和仿真验证了本文主动控制方法的有效性。

关键词：压电智能;宏观纤维复合材料;极点配置;闭环控制;有限元法